

# Direct assessment of living cell mechanical responses during deformation inside microchannel restrictions

Nadine Walter

Max Planck Institute for Intelligent Systems, Dept. New Materials and Biosystems & University of Heidelberg, Institute for Physical Chemistry, Dept. Biophysical Chemistry, Heisenbergstr. 3, D-70569 Stuttgart, Germany

Alexandre Micoulet

Department of Biomedicine, Unit for Nano-Featured Systems in Biomedicine, University of Bergen, Jonas Lies vei 91, 5009 Bergen, Norway

Thomas Seufferlein

Department of Internal Medicine I, Martin-Luther-University Halle-Wittenberg, Ernst Grube Str. 40, D-01620 Halle, Germany

Joachim P. Spatz<sup>a)</sup>

Max Planck Institute for Intelligent Systems, Dept. New Materials and Biosystems & University of Heidelberg, Institute for Physical Chemistry, Dept. Biophysical Chemistry, Heisenbergstr. 3, D-70569 Stuttgart, Germany

(Received 31 March 2011; accepted 22 July 2011; published 29 August 2011)

The deformation of suspended cells inside microchannel restrictions mimics passive cell transportation in the blood circulation system of the body. The cells traverse or get stuck in narrow vessels, as, e.g., during the metastasis of tumor cells. In this work, the mechanical responses of suspended pancreatic cancer cells as they move through and deform inside microchannel restrictions are assessed with a cantilever-based polydimethylsiloxane (PDMS) force sensor. Incorporated into a flow cell chip, the PDMS cantilever is integrated into the boundary wall of a narrow microrestriction. Upon being forced to enter the restriction by an applied flow, the cell exerts pressure on the cantilever, which then bends. By assuming a uniformly loaded cantilever, the total force and pressure on the cantilever can be calculated using elastic beam theory. This technique has the advantage of presenting an absolute and direct measure, which is independent of the applied flow and frictional processes at the channel–cell interface; in contrast to, e.g., measuring cell mechanics indirectly via cell sliding velocities. Furthermore, a high number of cells can be examined in a short time compared to other single cell mechanical testing devices. © 2011 American Vacuum Society. [DOI: 10.1116/1.3625258]

## I. INTRODUCTION

The living cell inside the body has to sustain physiologically relevant deformations and forces, both in the form of tissue deformation as well as on the single cell level. Tissue deformation can occur directly through macroscopic damage during an accident or indirectly through muscle contraction, which deforms surrounding tissues. Deformation on the single cell level is usually encountered when cells actively migrate through small gaps in the tissue or when they are driven through small capillaries in the blood circulation of the body. The latter situation mainly affects blood cells or, less commonly, tumor cells. Interestingly, mechanical resistance to deformation has been shown to correlate with the pathology of malaria-infected red blood cells.<sup>1</sup> In the same way, the mechanical properties of metastasizing tumor cells, which have acquired the ability to penetrate and infiltrate normal tissues to establish new tumors, might enhance or restrict tumor spreading. We describe a new microfluidic tool that allows the assessment of deformation forces and single cell resistance to deformation in a small confinement. Our device is able to mimic a vascular stenosis, while ena-

bling direct observation of the cell's mechanical resistance to deformation. This novel tool facilitates the differentiation between healthy and diseased cells according to their deformability, and thereby provides the basis for the development of diagnostic devices that have the potential to replace time-consuming laboratory analysis procedures.

The field of microfluidics lies at the interfaces among engineering, chemistry, and biology and has been used for a wide variety of applications and measurements, many of which aim to develop lab-on-a-chip systems. Only recently has microfluidics, which traditionally deals with the behavior and manipulation of fluids, been established as a tool for testing cell mechanics. In the used microchannel setups, cells can circulate in a controlled manner and can be manipulated individually. Examples of biophysical experiments using such setups include studies that look at cell dynamics and deformation on the single cell level during passage of the cell through a restriction in the channel. From these types of experiments, data on entry times, transit times, and transit velocities of the cell through the restriction can be obtained. These parameters are influenced by frictional forces ( $F_{\text{friction}}$ ), which are a function of the cell-exerted contact pressure ( $\sigma_{\text{contact}}$ ) and therefore influenced by the cell material properties during compression (see Fig. 1).

<sup>a)</sup>Electronic mail: spatz@is.mpg.de

Because several studies have shown that cell deformability can differ between healthy and diseased cells (see the following examples), such microfluidic measurements have broad utility for medical applications and clinical diagnostics. The detection of aberrant blood cells; for example, has been addressed in several studies. Shelby *et al.*<sup>1</sup> were able to show that malaria-infected red blood cells get stuck in restrictions more frequently than highly elastic healthy cells and describe a future application in drug screening. In their work, Rosenbluth *et al.*<sup>2</sup> demonstrated that both leukemia cells and white blood cells treated with cytoskeleton-affecting drugs have increased channel transit times in comparison to reference blood cells. These observations may explain microvascular obstructions like those observed during sepsis and leukostasis. Based on these findings a technique to identify patients with a high risk of developing leukostasis and a method to measure therapeutic efficacy may be developed in the future.<sup>2</sup> Similarly, white blood cells have been implicated in the obstruction of lung microvessels in acute lung injury. Using microchannel restrictions, Gabriele *et al.*<sup>3</sup> showed that both actin disruption and stabilization have a significant influence on the time needed by monocytes, a type of white blood cell, to squeeze into a channel and on their sliding velocity. Additional research on leukocyte deformability and rheology could eventually help solve clinically relevant problems during acute lung injury. Microfluidics could also bring forth great advances in cancer research, if a method can be developed that allows for differentiation between nonmalignant and malignant epithelial cells. Hou *et al.*,<sup>4</sup> in their study, showed that metastatic breast cancer cells enter into restrictions more easily than healthy cells, but slide with the same velocity through the channels. These examples demonstrate that optimizing microfluidic systems and their applications has the potential to create a broad range of clinically useful technologies and to promote the development of small-scale clinical diagnostic devices.

Based on the assumption that cell mechanics are different in healthy and diseased cells, all of the above-mentioned studies aimed to compare cells according to the mechanical properties of the cell membrane, i.e., the rigidity of the cell.

By measuring how quickly cells can travel through a restriction in the microfluidic capillary network, these studies used an indirect measure, namely channel transit time, to determine differences in cell mechanics. This approach has some disadvantages. Neither travel time nor velocity is a material constant, instead they represent functions of various experimental parameters. This results in a high susceptibility of the measurement to disturbances and makes comparisons across several experiments or between different microfluidic devices impossible. The following two examples illustrate how different experimental parameters can influence the sensitivity of these indirect measurements. One parameter that strongly affects cell travel time and velocity is the pressure throughout the flow field, which is susceptible to disturbances such as the presence of a cell. The flow pressure drives the cell into and through the microrestriction, and as the cell changes its shape during microrestriction passage flow conditions are modified in an unpredictable and immeasurable way. Another influential parameter is the contact pressure that the cell exerts on the channel wall. As a rule, frictional forces should increase as the contact pressure between the cell and the channel surface becomes stronger, and slow down the cell. Instead, a brushlike cell surface or the fluid layer in between the cell and the channel wall, to name two examples, can counteract these frictional forces.

To overcome the measurement uncertainties inherent to an indirect measurement of cell mechanics, we developed an absolute and direct method for the quantification of cell deformation resistance inside microchannel restrictions. Here we demonstrate its applicability using suspended pancreatic cancer cells (Panc-1).

The physiology and mechanics of the suspended state of usually adherent cells is under-researched, as most cell functions depend on surface attachment. In the case of cancer metastasis; however, cells detach once they have reached the circulation system and must be able to survive autonomously.<sup>5</sup> In order to measure cell deformation resistance, a flexible elastic flap was incorporated into the microchannel restriction of a microcanal setup. This flap serves as a deformation sensor when the cell is compressed inside the restriction (see Fig. 2).

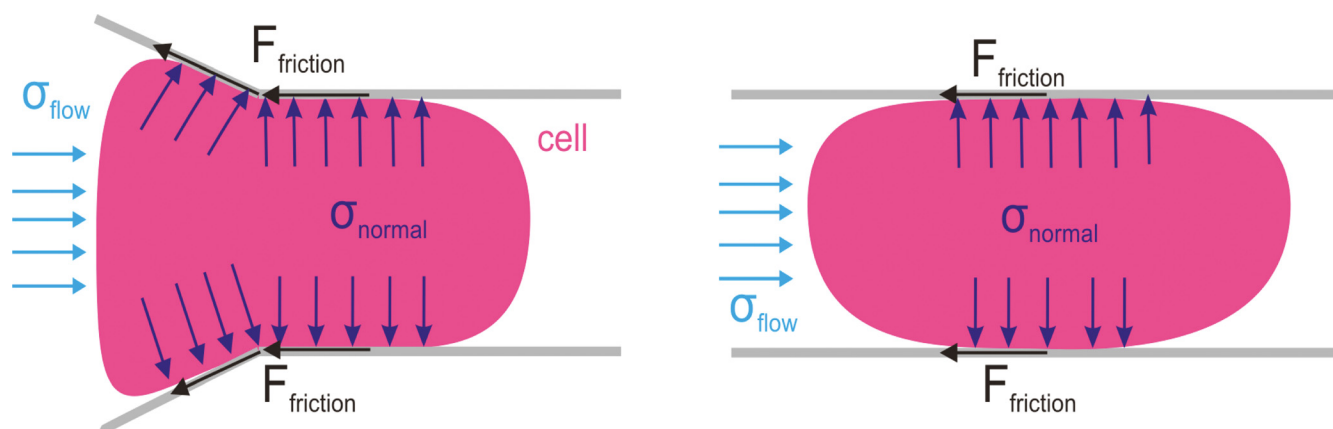


FIG. 1. (Color online) Sketch of pressure distributions originating from flow ( $\sigma_{\text{flow}}$ ) and cell deformation resistance ( $\sigma_{\text{normal}}$ ), as well as frictional forces ( $F_{\text{friction}}$ ) that are present when a cell enters (left) and transits (right) a microrestriction.

The use of a flexible flap to assess cell mechanics represents a novel application, although similar flaps have been used as microfluidic diodes<sup>6</sup> and flow rate sensors.<sup>7</sup>

We introduce the use of a polydimethylsiloxane (PDMS) cantilever as a cell mechanics sensor and exemplify its mode of operation by measuring cell deformation dynamics during fast cell deformation in a 2D confinement and the forces exerted by cells on the channel walls. The technique is discussed in comparison to other cell mechanics probing techniques that can be applied to suspended cells like the optical stretcher<sup>8</sup> and micropipette aspiration<sup>9</sup> and suggestions for further improvements and applications are given.

## II. MATERIALS AND METHODS

### A. Cell culture and suspended cell characteristics

Pancreatic cancer cells (Panc-1) (Ref. 10) were chosen as an example of an epithelial cancer cell line. Panc-1 cells were cultured in DMEM (Gibco) with 10% FCS (PAA Labs) up to 70% confluency at 37 °C with a 5% CO<sub>2</sub> atmosphere. Panc-1 cells, like all adherent cells, normally show spreading on a 2D cell culture flask. In order to obtain suspended cells, the cells were detached from the surface by trypsin treatment, which destroys cell to surface bonds enzymatically. After trypsination of cells, they were diluted in fresh medium and applied to the microchannel after at least 1 h.

Because the cell shape as well as the development of cytoskeletal elements can differ greatly between the adherent and the round suspended cell state, we determined several cell-specific parameters before employing the cells in microchannel experiments. The cell diameter must be known for these types of experiments, as it determines the appropriate channel and microrestriction size. Prior to entering the restriction the cells should be compressed only between the

top and bottom sides of the channel, but upon entering it the cells are deformed with a predefined compression ratio, which depends on the cell diameter. The mean cell diameter of the spherical suspended Panc-1 cells was determined to be 22.5 ( $\pm 3.8$ )  $\mu\text{m}$  from light microscopic images [see Fig. 3(a)]. As research has shown the nucleus to be a great deal stiffer than the cytosol of the cell,<sup>11</sup> we measured the size of the nucleus before commencing measurements. Utilizing light microscopic images of spread cells we approximated the nucleus as an ellipsoid and determined the length of a mean long and a mean short axis (both presumed to be normally distributed), to be 23.0 ( $\pm 7.8$ ) and 18.2 ( $\pm 4.9$ )  $\mu\text{m}$ , respectively [see Fig. 3(b)]. These dimensions represent an upper limit for the nucleus size, because in the adherent state of the cell the nucleus is stretched and extended by cytoskeletal fibers.<sup>12</sup> During the suspended cell state, cells commonly store excess surface area in membrane wrinkles, which can be utilized to resist rupture during deformation. We determined the Panc-1 cells to have an approximate 3.3 ( $\pm 0.1$ )-fold surplus of membrane area in the round state. Using volume conservation and assuming the cell to deform from a spherical shape to a cuboid one, it is estimated that Panc-1 cells can squeeze into channels down to a size of 4.5  $\times$  4.5  $\mu\text{m}$  without rupturing. Further, Panc-1 cells can be multinucleate; in other words, they can contain more than one nucleus per cell.

### B. Design of the flow cell and microchannel restriction including the force sensor

The flow cell chip consists of 16 parallel channels, which open out into a common reservoir at each end, as depicted in Fig. 4. Using a construction with several channels offers the opportunity to fall back on other channels if one is blocked.

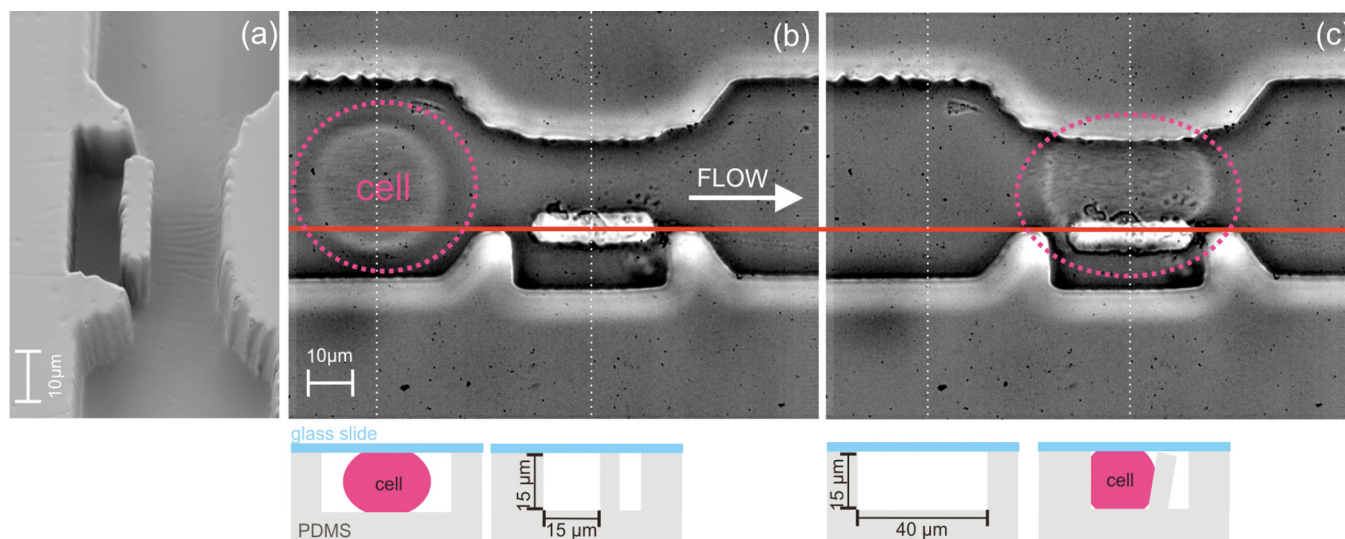


Fig. 2. (Color online) Direct assessment of cell mechanics via a cantilever-based PDMS deformation sensor inside a microchannel restriction. (a) Scanning electron micrograph of the microflap restriction (left) photographed from above at an angle of approximately 30°. (b) Top: view of cell approaching restriction equipped with cantilever from above (through glass slide); below: sketch of channel cross sections when cell is approaching restriction (left: in front of restriction, right: restriction). (c) Top: view of cantilever with deformed cell and bent microflap from above; below: sketch of channel cross sections while cell is passing restriction (left: in front of restriction, right: restriction).

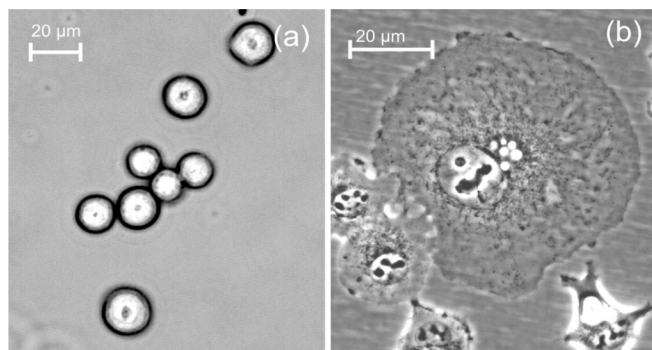


FIG. 3. Pancreatic cancer cells (Panc-1). (a) Suspended round cells. (b) Adherent cell which spreads flat on the substrate. The ellipsoidal nucleus is situated near the middle of the cell.

The individual channels are  $15\ \mu\text{m}$  high and  $40\ \mu\text{m}$  wide and incorporate one microflap containing restriction each, which is situated equidistant to the reservoirs. The restriction itself consists of a rectangular shaped channel (with one side provided by the microflap) that has an equal width and height of  $15\ \mu\text{m}$  and a length of  $25\ \mu\text{m}$ . The PDMS microflap measures  $5\ \mu\text{m}$  in thickness ( $T$ ),  $15\ \mu\text{m}$  in length ( $L$ ), and  $25\ \mu\text{m}$  in width ( $W$ ). The geometry of the microflaps; in other words, the size and shape, was kept constant for all experiments (compare Fig. 4).

### C. Flow cell production

PDMS is a material that is commonly used for microfluidics processing and is highly suitable for use in our microflap incorporated force sensor, because its elastic properties are adjustable.<sup>13</sup> The flow cell chip negative SU-8 (SU-8-2025, Microchem) mask for the microrestrictions and the flap was produced in one step using standard photolithographic techniques.<sup>3</sup> PDMS (Sylgard 184 Elastomer Kit, Dow Corning) with a 15:1 base to crosslinker ratio was poured on the mold and cured at  $80\ ^\circ\text{C}$  for 2 h. After having cooled down to room temperature, the flow cell

was peeled off the mold under ethanol immersion. Although the degree of wetting between PDMS and ethanol is very high, this step remains critical due to the risk of the flap sticking and rupturing. Subsequently, holes were punched in the two reservoirs and the PDMS was bonded to a glass cover slip using oxygen plasma. Fortunately, the flap does not stick to glass, presumably because of the small contact area and contact pressures. Tubing was inserted in the reservoirs and sealed with PDMS and glue.

### D. Experimental procedure

Prior to experiments, the cells from a well (growth area approximately  $9.5\ \text{cm}^2$ ) with a 70% confluent adherent cell culture were trypsinized and resuspended in 1 ml cell culture medium. The cells were kept in suspension in a tube for 20 min at  $37\ ^\circ\text{C}$  and 5%  $\text{CO}_2$  to recover. Afterwards, the cells were resuspended, aspirated with a 1 ml syringe, and immediately used for experiments. In our experiments a constant total volume flow rate ( $f_{\text{total}}$ ) of  $5\ \mu\text{l}/\text{min}$  was induced through the parallel channel system by a syringe pump (PHD 2000, Harvard Apparatus). Utilizing volume conservation and symmetric geometry, we roughly determined the resulting local flow rate through the restriction to be approximately  $312\ \text{nl}/\text{min}$ , which equals  $f_{\text{total}}/16$ . The exact measurement of local flow rates and pressures exerted on a cell in microrestrictions is impossible in microfluidic setups such as this one, because of the unknown and dynamic cell geometry during the cell squeezing process. The fact that some parameters, which directly affect cell sliding velocities, can only be estimated, again highlights the disadvantages of indirect cell mechanic measurements. During the experiments, the flow cell chip and the syringe were kept inside a heated incubation chamber at  $37\ ^\circ\text{C}$  on an optical microscope (Axiovert 200, Zeiss), utilizing a high magnification objective ( $100\times$ , Zeiss). A high-speed camera (Phantom V, Vision Research Inc.) recorded cantilever deflection and cell deformation events. The final recording time took less than 1 min.

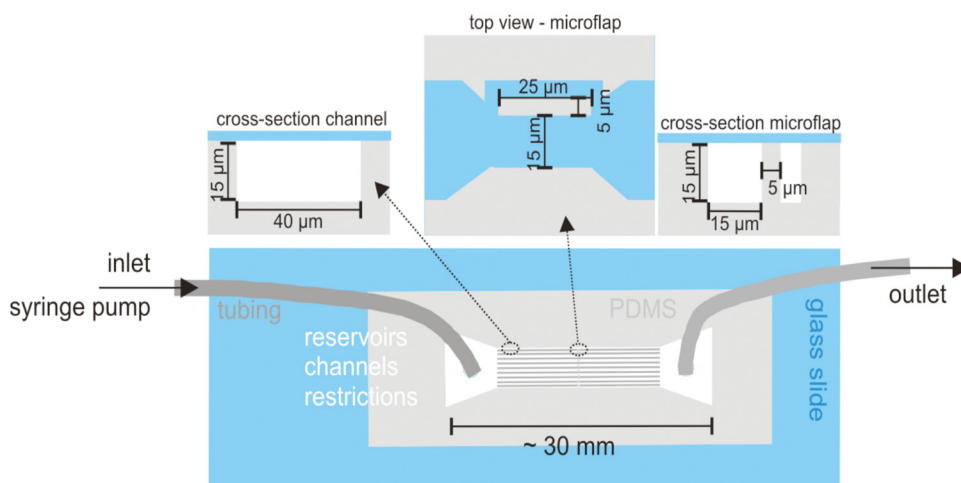


FIG. 4. (Color online) Sketch of the flow cell chip and microflap restriction.

### E. Tracking of the PDMS cantilever bending

A customized MATLAB (The Mathworks Inc.) routine detected the outer edge of the flap by finding intensity minima in line profiles perpendicular to the flow direction, as depicted in Fig. 5. Deflection resolution is principally restricted by the pixel size of the camera and the optical resolution of the objective plus microscope. Although the standard deviation during flap bending exceeded the standard deviation without bending by 1 pixel, suggesting a systematic error, bending due to cell transit was resolved sufficiently. The microflap torsion was not significant during cell deformation and cell passage.

### F. Force approximation for a uniformly loaded cantilever

As the microflap has a known geometry and consists of an elastic material, elastic beam theory can be applied to correlate deflection and exerted force. Because the cell completely fills the restriction volume and adjusts its shape to the channel, we assume uniform loading with an evenly distributed constant contact pressure on the flap area [ $P$  (N/m<sup>2</sup>)] and a constant force per length [ $f$  (N/m)] (see Fig. 6). These approximations allow the calculation of the absolute force that a cell exerts on the rectangular PDMS flap with known width ( $W$ ), length ( $L$ ), and thickness ( $T$ ). However, the occurrence of nonuniform loading conditions originating from inhomogeneities, such as the nucleus, cannot be excluded. Thus, the calculated forces should be regarded as approximations.

For a uniformly loaded beam, the absolute value of the locally applied torque,  $M(x)$ , must be balanced by the elastic energy of the beam,

$$M(x) = \frac{EI}{R(x)}. \quad (1)$$

The stored elastic energy is dependent on the elastic modulus of the beam material ( $E$ ), the area moment of inertia ( $I$ ), and

the local beam curvature [ $1/R(x)$ ]. Furthermore, for small deformations of the flap fixed at the end, the beam curvature can be described as the second derivative of the beam shape,

$$\frac{1}{R(x)} \approx \frac{d^2y}{dx^2}(x). \quad (2)$$

Using Eqs. (1) and (2), integration leads to the beam shape and the deflection at length  $L$ ,<sup>14</sup>

$$y(x) = \frac{1}{EI} \int \left[ \int M(x) dx \right] dx, \quad (3)$$

$$y(L) = \frac{3}{2} \frac{fL^4}{ET^3W}. \quad (4)$$

Here, the applied torque [ $M(x)$ ] at a point on the beam originating from the uniform load per length ( $f$ ) is given by

$$M(x) = \int f(L-x) dx. \quad (5)$$

The area moment of inertia ( $I$ ) for a rectangular beam is constant over the beam length and is given by

$$I = \frac{T^3W}{12}. \quad (6)$$

Knowing the cantilever end deflection, the total force on the flap ( $F$ ) and the exerted pressure ( $P$ ) can be obtained as follows:

$$F = fL = \frac{2y(L)ET^3W}{3L^3}, \quad (7)$$

$$P = \frac{f}{W} = \frac{F}{WL} = \frac{2y(L)ET^3}{3L^4}. \quad (8)$$

The microflap geometry was determined by scanning electron microscopy (SEM), as well as optical microscopy. The PDMS elastic modulus was determined via indentation testing.

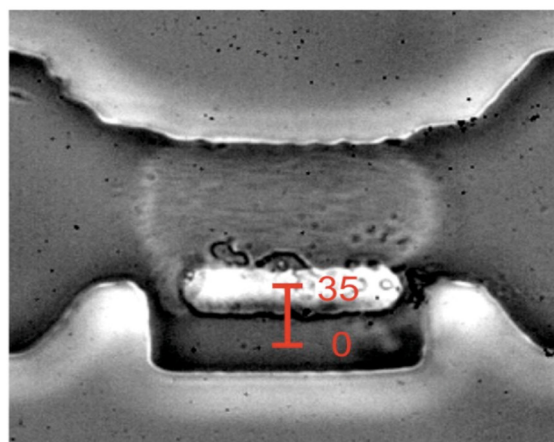
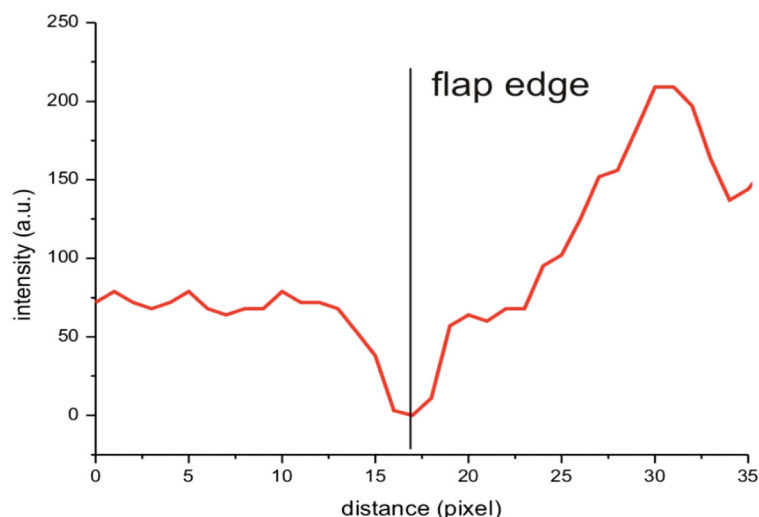


FIG. 5. (Color online) Flap deflection (left) was tracked via minimum intensity edge detection in line profiles perpendicular to the flow direction (right).

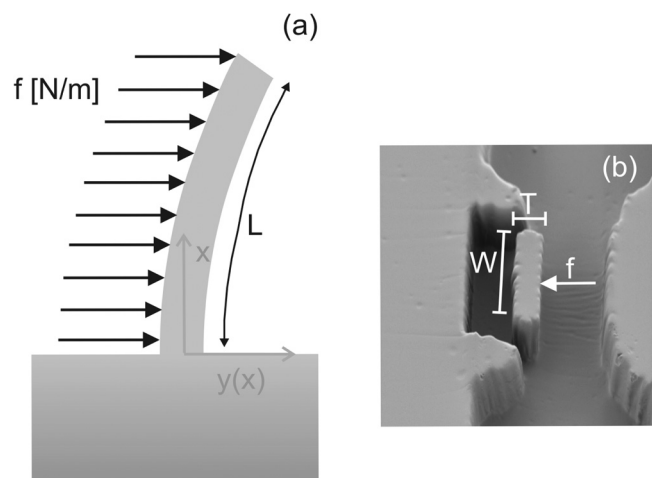


FIG. 6. (a) Sketch of cross section of a uniformly loaded microflap and (b) SEM picture of microflap from an angle of approximately 30° toward the y-z-plane:  $L$  = length,  $W$  = width,  $T$  = thickness of flap,  $f$  = force per length of flap.

**G. Determining the PDMS elastic modulus with atomic force microscopy**

The PDMS elastic modulus was determined with spherical indentation testing using an atomic force microscope (MFP-3D, Asylum Research). The flow cell, which is basically a thick PDMS sheet, was indented a few hundred nanometers in

de-ionized water using glass spheres with radii of 4–4 μm (SPI supplies and Worf Glaskugeln, Germany) glued to tipless atomic force microscopy (AFM) cantilevers (TL-FM, Nano and More) with a nominal spring constant of 2 N/m. The Hertz model<sup>14–16</sup> for a rigid spherical indenter and a Poisson ratio of 0.5 for PDMS was fitted to the force-indentation curves revealing elastic moduli between 0.7 and 1.1 MPa for different PDMS batches of a 1:15 base to crosslinker ratio. Concentration errors, curing, and aging effects are assumed to be the reasons for the variation between the batches. The relative error of the PDMS elastic modulus of a specific flow cell was estimated at 20% and mainly due to cantilever calibration using a reference cantilever.<sup>17,18</sup>

**III. RESULTS**

**A. Measurement of single cell dynamics through microflap restriction**

A single cell event is recorded where a cell is traversing the microflap restriction. The flap end deflection [ $y(L)$ ] as well as the cell length ( $L_{cell}$ ), which is defined as the difference of cell front and cell back edge coordinates, was tracked over time. Figure 7 shows the data and the corresponding optical images of the deformation of the cell inside the restriction. A maximum deflection of the flap [ $y(L)_{max}$ ] is reached, as the cell is nearly situated in the middle of

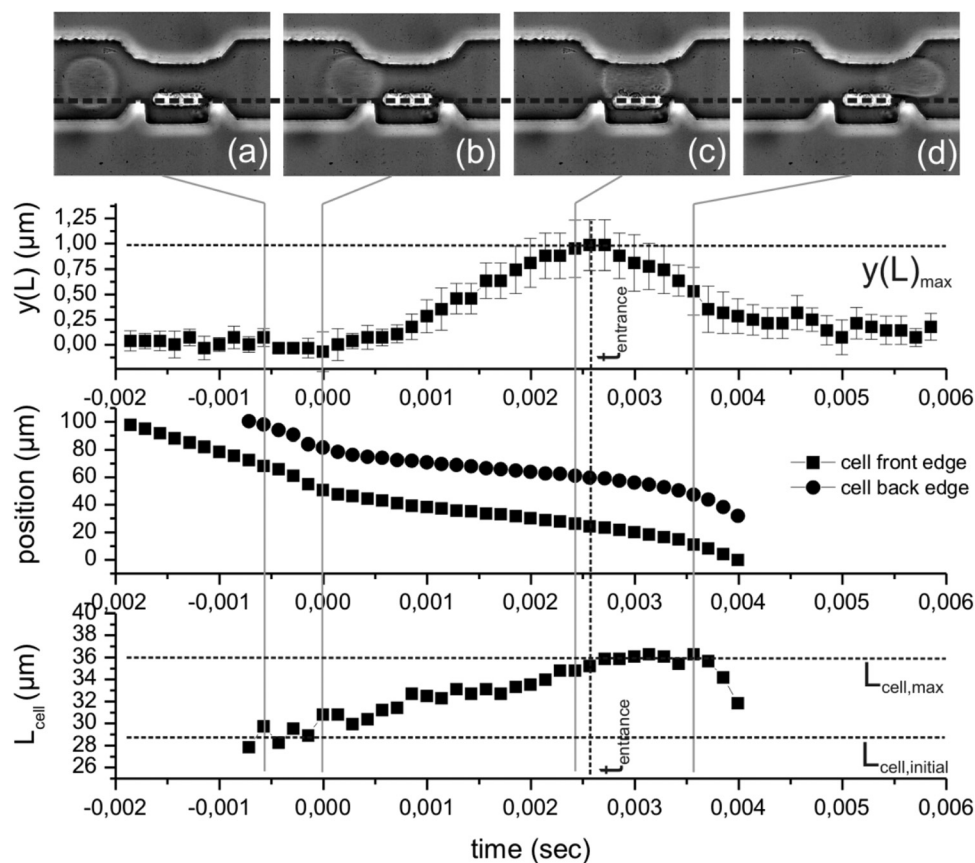


FIG. 7. Single cell dynamics. Flap deflection  $Y(L)$ , cell front and back edge position as well as cell length  $L_{cell}$  are plotted over time. (a) The cell approaches the restriction. (b) The cell starts to enter the restriction. (c) The cell is completely compressed. (d) The cell exits the restriction.

the restriction. The maximum cell length ( $L_{cell,max}$ ) coincides with the maximum deflection. The initial cell diameter ( $L_{cell,initial}$ ) of the undeformed, and thus perfectly spherical, cell before entering the restriction can be deduced from the data and is marked with a spotted line in the bottom graph. The amount of time it takes the cell from the initial contact with the restriction until maximum flap deflection (which coincides with the cell acquiring maximum length) is defined as the entrance time ( $t_{entrance}$ ). In addition, the mean cell approach velocity and the mean cell sliding velocity through the restriction can be obtained from the graph (not shown).

**B. Correlation between microflap deflection and cell mechanical properties**

To identify possible correlations, the maximum deflection of the flap [ $y(L)_{max}$ ], the maximum cell length ( $L_{cell,max}$ ), and the entrance time ( $t_{entrance}$ ) were plotted for five single cell passages as a function of initial cell length ( $L_{cell,initial}$ )

[Figs. 8(a)–8(c)]. Assuming that a cell with high water content is incompressible, we can apply the principle of mass conservation to the volume of the cell, to predict that a more voluminous cell will stretch out longer than a less voluminous cell inside a fixed geometry. Thus, it is not surprising that  $L_{cell,initial}$  positively correlates with  $L_{cell,max}$  [see Fig. 8(b)]. Due to the fact that cells consist of a homogeneous and mainly linear viscoelastic material, the larger a cell is the greater the force required to compress the cell into a microrestriction with a defined size. Therefore, a positive correlation between cell size and  $y(L)_{max}$  can be expected. Interestingly, the data of five single cell passages show ambiguity here [see Fig. 8(a)]. This either suggests a variability in the mechanical properties among the different cells or differences in the flap loading conditions arising from sub-cellular inhomogeneities of, e.g., the nucleus. When including all measured values of an experiment (both values obtained from often occurring rows of multiple cells and values from less frequent single cells), however, the maximum deflection [ $y(L)_{max}$ ] positively correlates with the cell

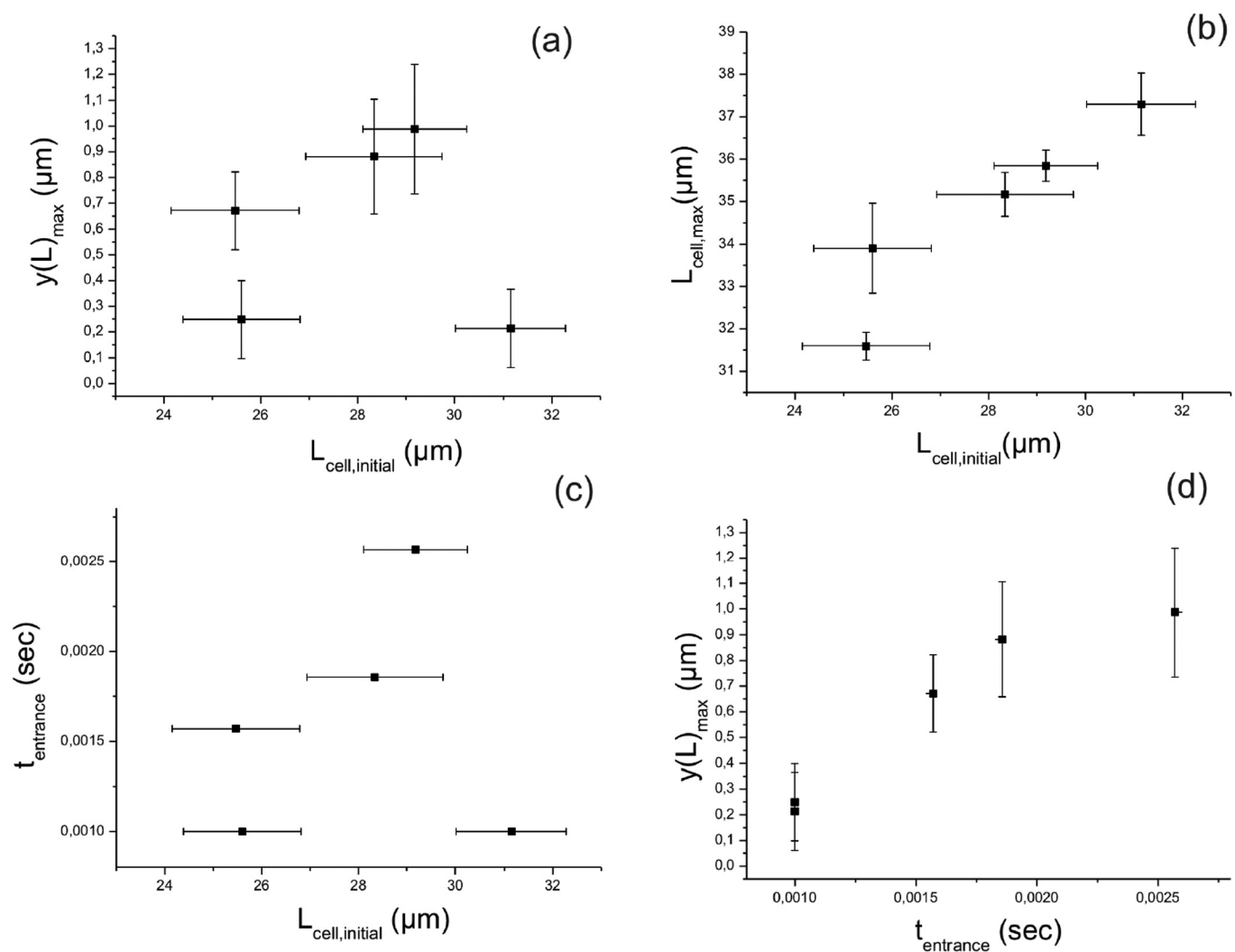


FIG. 8. (a) Maximum flap deflection over initial cell diameter. (b) Maximum cell length over initial cell diameter. (c) Entrance time over initial cell diameter. (d) Entrance time over maximum flap deflection.

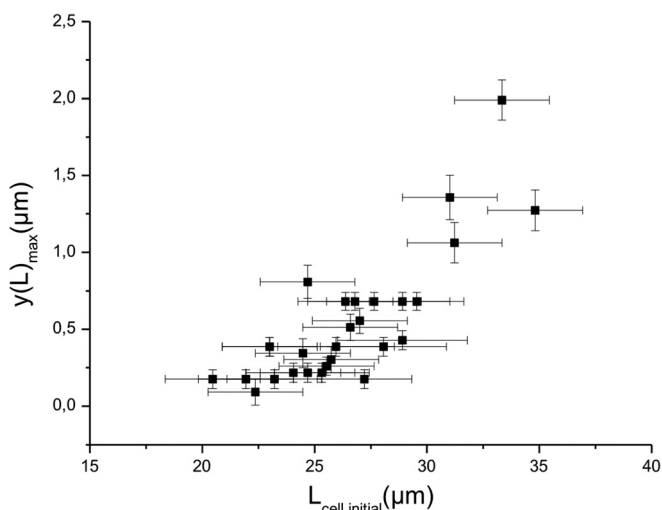


FIG. 9. Initial cell length over maximum flap deflection for different sized cells of one population. Data are taken from one experiment.

size (see Fig. 9). The data show that the observed cells exhibit both viscous and elastic characteristics when undergoing deformation. Again, the data scatter can be attributed to cell inhomogeneity or different loading conditions. In the case of  $y(L)_{\max}$  and the entrance time ( $t_{\text{entrance}}$ ), an unambiguous assignment of the values to the cell volume is not possible [see Figs. 1(c), 8(a), and 8(c)]. However, a direct correlation was found between  $y(L)_{\max}$  and  $t_{\text{entrance}}$  (the time it takes the cell to squeeze into the restriction) [see Fig. 8(d)]. This is a direct proof that the entrance time actually reflects normal forces that a cell exerts in narrow restrictions.

### C. Forces and pressures exerted by the cells

Assuming a uniform loading by the cell, meaning that the cell-exerted pressures are distributed uniformly across the cantilever area, the total force and pressure exerted by the cell can be calculated from the maximum end deflection of the microflap [ $y(L)_{\max}$ ], the elastic modulus ( $E$ ), and the geometry of the PDMS microflap ( $W$ ,  $L$ ,  $T$ ) by applying Eq. (7). Figure 10 shows how the absolute measured forces of two experiments using two different flow cell chips compare. The absolute measured forces were obtained by plotting the initial cell diameter ( $L_{\text{cell,initial}}$ ) against the total maximum force ( $F$ ) that is applied on the flap by each cell that passes through the restriction. The absolute measured force is necessary for comparing different experiments on several flow cell chips, because the PDMS elastic moduli vary for each batch of PDMS used for flow cell production (see Sec. II). The total forces that cells exert on the microflap range from 50 to 1250 nN, which lies in the force range of what is obtained by AFM compression testing (data not shown). Absolute force errors are determined by deflection resolution, which is the standard deviation, errors in the elastic modulus, and flap dimensions. Total pressures exerted by

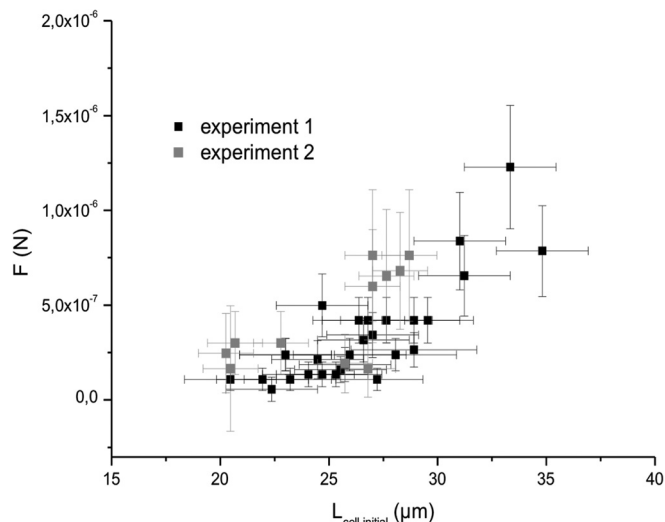


FIG. 10. Initial cell length over maximum applied force for different sized cells of one population. Data are taken from two independent experiments.

the cells, obtained by applying Eq. (8), range from  $\approx 100$  to 3000 Pa.

## IV. DISCUSSION

This paper introduces a novel cantilever-based method to assess the cell deformation response of round cells in microrestrictions. Cantilever deflection and forces as well as the corresponding cell-exerted pressures represent an absolute and direct measure of the cell mechanical response. Apart from enabling interesting basic research in the form of physiological cell response measurements during 2D compression, this new method has the potential to be developed into a high-throughput testing tool for cell mechanics.

In this paper we were able to measure cell deformation responses that allow the calculation of nanonewton scale absolute forces that passing cells exert on a microrestriction wall. This method allows the comparison of whole cell populations under constant experimental conditions and is able to detect differences in cell size and cellular homogeneity. We found the maximum deflection to positively correlate with the cell size, which speaks for a partly elastic cell mechanical behavior. Nevertheless, cell mechanical responses are highly complex and also depend on other factors, such as deformation rates, deformation ratios, as well as the geometry of the deformation. In addition, cell mechanical behavior depends on the cell type: whether the suspended cells show a more viscous or a more elastic behavior and/or whether the cells are prone to fluidization at a critical deformation rate. Our setup is able to obtain absolute forces regardless of such variability among the measured cells.

The microflap we employed in our experiments is able to measure both forces and relaxation processes, but absolute force measurements require knowledge of the loading conditions of the microflap. For the simple case of a uniform

load, total force and pressure were calculated in this paper. Nevertheless, there is room for improvement; for example, by increasing the deflection and force resolution of the cantilever-based measurement. This could be achieved by: (1) a decrease in thickness and width of the microflap, (2) an increase in flap length, (3) by using PDMS with a lower elastic modulus (4) or through replacement of PDMS with another suitable soft material. However, until now the limiting factor continues to be the peel-off process of the delicate flaps during production, which therefore restricts modification of the microflap. Another way to achieve resolution up to the nanometer scale could be through the employment of a laser-assisted method for image processing, such as is used in atomic force microscopy.

A direct comparison to other techniques that can be used to measure the viscoelastic properties of cells reveals the benefits and drawbacks of using a microflap. A clear advantage to micropipette aspiration,<sup>9</sup> for example, is the fact that the microflap setup has the potential to be developed into a high-throughput tool. Because it is quite simple and inexpensive to fabricate and reproduce, it is very amenable to mass production. In contrast, using a microflap presents disadvantages when compared to, for example, the optical stretcher.<sup>8</sup> The optical stretcher uses a tunable laser to trap and deform cells between two counterpropagating beams generated by the laser and thereby measures cell deformation. In contrast, the microflap is a contact-based mechanical testing system with a fixed geometry, which must be adjusted to the desired compression ratio for different cell types. Furthermore, this setup is susceptible to artifacts caused by cell trash, agglomerations of cells, and multiple cells, although this may be avoided by thorough mixing of the cell suspension and the application of flow focusing.

In summary, this technique introduces great improvements for the exact measurement of absolute deformation forces and holds promise for advancing the development of clinically useful devices for detecting cell mechanical differences between healthy and diseased cells. In addition, this method may prove to be applicable for measuring vesicles or soft elastic beads in the future.

## ACKNOWLEDGMENTS

The authors especially acknowledge Subra Suresh (MIT, NSF), who has substantially guided and inspired the research presented here. The authors also acknowledge Kristen L. Mills, Iain Dunlop, Tamas Haraszti, and Nina Grunze for discussion and manuscript improvements. Financial support by the Deutsche Krebshilfe e. V. and the Max Planck Society is highly appreciated. Part of the research leading to these results has received funding from the European Union Seventh Framework Programme (FP7/2007-2013) under Grant Agreement No. NMP4-LA-2009-229289 NanoII. J.S. is a Weston Visiting Professorship at the Weizmann Institute of Science, Israel.

<sup>1</sup>J. P. Shelby, J. White, K. Ganesan, P. K. Rathod, and D. T. Chiu, *Proc. Natl. Acad. Sci. U.S.A.* **100**, 14618 (2003).

<sup>2</sup>M. J. Rosenbluth, W. A. Lam, and D. A. Fletcher, *Lab Chip* **8**, 1062 (2008).

<sup>3</sup>S. Gabriele, A. M. Benoliel, P. Bongrand, and O. Theodoly, *Biophys. J.* **96**, 4308 (2009).

<sup>4</sup>H. W. Hou, Q. S. Li, G. Y. H. Lee, A. P. Kumar, C. N. Ong, and C. T. Lim, *Biomed. Microdevices* **11**, 557 (2009).

<sup>5</sup>P. Gassmann and J. Haier, *Clin. Exp. Metastasis* **25**, 171 (2008).

<sup>6</sup>M. L. Adams, M. L. Johnston, A. Scherer, and S. Quake, *J. Micromech. Microeng.* **15**, 1517 (2005).

<sup>7</sup>J. Loverich, I. Kanno, and A. Kotera, *Microfluid. Nanofluid.* **3**, 427 (2007).

<sup>8</sup>J. Guck *et al.*, *Biophys. J.* **88**, 3689 (2005).

<sup>9</sup>R. M. Hochmuth, *J. Biomech.* **33**, 15 (2000).

<sup>10</sup>M. Lieber, J. Mazetta, W. Nelson-Rees, M. Kaplan, and G. Todaro, *Int. J. Cancer* **15**, 741 (1975).

<sup>11</sup>N. Caille, O. Thoumine, J. Tardy, and J. J. Meister, *J. Biomech.* **35**, 177 (2002).

<sup>12</sup>J. P. Jean, D. S. Gray, A. A. Spector, and C. S. Chen, *J. Biomech. Eng.* **126**, 552 (2004).

<sup>13</sup>M. J. Madou, *Fundamentals in Microfabrication* (CRC Press, Boca Raton, FL, 1997).

<sup>14</sup>L. D. Landau and E. M. Lifshitz, *Theory of Elasticity* (Elsevier Butterworth-Heinemann, Oxford, 2005).

<sup>15</sup>H. Hertz and *J. Reine Angew. Math.* **92**, 156 (1881).

<sup>16</sup>I. N. Sneddon, *Int. J. Eng. Sci.* **3**, 47 (1965).

<sup>17</sup>A. Torii, M. Sasaki, K. Hane, and S. Okuma, *Meas. Sci. Technol.* **7**, 179 (1996).

<sup>18</sup>J. P. Spatz, S. Sheiko, M. Möller, and O. Marti, *Langmuir* **13**, 4699 (1997).